Intraplate seismicity in NW Iberia along the trace of the Ventaniella Fault: a case for fault intersection at depth

López Fernández, Carlos (*)

Fernández-Viejo, Gabriela

Olona, Javier

Llana-Fúnez, Sergio

(*) Corresponding author: Department of Geology, C/ Arias de Velasco s/n, 33.005 Oviedo (Spain). Phone: +34 985103110. E-mail: lopezcarlos@uniovi.es

ABSTRACT

Intraplate seismicity in NW Spain, an otherwise stable continental area, is dominated by low magnitude events and occurs both in swarms or dispersed along faults. A detailed study of one of the most active fault segments, the Ventaniella Fault, has produced an accurate image of foci distribution and revealed new insights on the origin of this lingering activity. The improved location of earthquakes by a temporary seismic network has allowed to better constrain the geometry of the seismogenic segments of the fault at depth.

Between 2015 and 2017, a portable seismic array of 10 seismographs recorded 45 low magnitude earthquakes (<2) at depths between 9-18 km. These hypocenters define a tubular trend plunging to the northwest. The linear seismicity pattern is interpreted as the result of the intersection at depth of two main fault planes: a NW-SE fault reactivated in the Alpine Orogeny and the frontal thrust of the Cantabrian Mountains running E-W. The clustering of earthquakes along this particular line of intersecting faults coincides spatially with the presence at depth of an important lateral gradient in crustal thickness, related to the termination of the crustal root beneath the Cantabrian Mountains. The mechanical constraints in the continental crust imposed by the arrangement of crustal scale faults and the gradient in crustal thickness may have reactivated seismically old faults in a context of a stable continental area.

Key words: intraplate seismicity, fault intersection, Ventaniella Fault, Cantabrian Mountains Front, local seismic network, lateral Moho gradient.

INTRODUCTION

The northwest corner of the Iberian Peninsula is considered a relatively low-seismicity intraplate zone (Custodio et al., 2015; López-Fernández et al., 2004, 2012; Martínez-Díaz et al., 2006; Mezcua et al., 2011), located hundreds of kilometers away from the current active African-Eurasian plate boundary (Figure 1). The presence of seismic stations there in the national network is therefore sparse. The seismicity record shows a dispersed spatial distribution, so even when there have been earthquakes in historical time, little attention has been paid to their analysis.

Intraplate seismicity, in general, does not receive as much attention as plate boundary related activity, given the longer return periods of hazardous events (e.g. Johnston, 1989; Stein and Liu., 2009). However, there are well known cases of intraplate earthquakes large enough to produce serious damage in areas that are relatively badly prepared to deal with their resulting ground motions (e.g. Bent, 1994; Calais et al., 2016; Johnston, 1996; Mishra et al., 2014; Satyabala, 2006; Schulte and Mooney, 2005). The origin of intraplate seismicity is not straitghtforward as in plate boundaries; it has been attributed to fault intersection (e.g. Gangopadhyay and Talwani, 2005; Sibson, 1988; Talwani, 1989), differential strength at depth transferred upwards (Kenner and Segall, 2000; Liu and Zoback, 1997; Qingsong et al., 2007; Sandiford and Egholm, 2008) and sometimes to hydrological causes (eg. Bollinger et al., 2010; Costain, 2008; Costain et al., 1987; Wolf et al., 1997). Some studies have suggested that there is a preference for intraplate earthquakes to occur in regions of inherited rifted crust, compared with non-rifted margins (e.g. Johnston et al., 1994). However Schulte and Mooney (2005) concluded that, on a global scale, the correlation between intraplate earthquakes and rifted crust has been overestimated, with factors such as stretching ratios in the pre-rift process and flexural effects from a thick sedimentary load being more important than solely the rifted nature of the crust. Nonetheless, the original cause of intraplate seismicity remains poorly known in many areas and some combined mechanisms of reactivation of old structures and/or deep seated processes are invoked to produce the mechanical weakening of limited areas in otherwise stable crust. Intraplate seismicity can help elucidate the dip and depth of mapped structures at the surface that elude interpretation in seismic reflection data due to its verticality or in seismic refraction and gravity.

In general, in the NW Iberian Peninsula, earthquake magnitudes are below 3.5 (Martínez-Díaz et al., 2006; López-Fernández et al., 2012; Martín-González et al., 2012). In the Atlantic sector, the activity is concentrated in "earthquake swarms", that generally show a subvertical tubular or pipe-like shape from the surface to around 12-15 km in depth (López-Fernández et al., 2012; Martín-González et al., 2012; Llana-Fúnez and López-Fernández, 2015). The largest of these is the so-called Becerreá swarm (Figure 1). Since 1979 seven seismic sequences were recorded in that swarm, including a main event (21 May 1997) of magnitude 5.1 m_bLg ($m_bLg = \log[A/T]+1.05\log \Delta+3.90$; being A the amplitude in micrometers and T the period in seconds of the sustained maximum of the wave train Lg, and Δ the epicentral distance in degrees.), the largest instrumental earthquake recorded in this region. The base of the seismogenic zone in this part of Iberia ranges between 19 and 20 km being shallower in the Becerreá swarm (16-17 km), possibly related to the effect of local high geothermal gradients and the presence of pressurized fluids within the crust (Llana-Fúnez and López-Fernández, 2015).

In the Spanish Atlantic sector, earthquakes are associated to NW-SE and NNE-SSW dominant faults and seismicity in the Becerreá swarm has been related directly to NNE trending strike-slip faults (González-Casado and Giner, 2000; Martínez-Díaz et al., 2006). The intersection of subvertical faults was proposed by López-Fernández et al. (2012) to explain the vertical pipe-like earthquake swarms.

Away from the Atlantic rim, in the central part of the Cantabrian Mountains and adjacent Cantabrian Margin, the events are more sparse. One of the most significant earthquake alignments partially follows the southern inland trace of the Ventaniella Fault (Figure 1). This fault records a complex and multiphase tectonic evolution. Striking NW-SE, its mapped trace runs for more than 400 km, including its offshore prolongation within the margin continental platform, where it is also known as the Cantabrian Fault (Viejo et al., 2014). Data provided by the Spanish seismic network (SSN, see Data and Resources Section) and from López-Fernández et al. (2004), indicate that this fault only presents persistent seismicity over an inland southern segment 70 km long, coinciding with the elevated parts close to the watershed in the Cantabrian Mountains (Figure 1). This activity is sporadic, of low magnitude, but with depths that reach almost 20 km.

The biggest instrumental earthquake in the area corresponds to an m_bLg 3.7 event that occurred on 02/20/1989 (Figure 1). Historical accounts of large events, near the Cantabrian and Ventaniella Faults, are found in the literature (eg. Martínez-Solares and Mezcua, 2002; Díaz-Díaz, 2016). For instance, in 1522 an earthquake produced significant damages in the city of Avilés; in 1861 and 1877 local records locate the epicenter to the NW of this city, while another earthquake was intensely felt in 1846 at Peñas Cape (location in Figure 1). The historical and current seismicity and the presence of active quaternary faults in the region (Nozal and Gracia, 1990; Gutiérrez Claverol et al., 2006) are indicative of continuous lingering tectonic activity.

Being a relatively quiet area within the Iberian Peninsula, the Spanish Seismic Network (SSN) with only two stations nearby (Figure 1), lacks a detailed resolution of the seismicity there. Therefore, to obtain a more precise image of this low magnitude, persistent seismicity a temporary seismic network was deployed between September 2015 and March 2017 around the southeastern part of the Ventaniella Fault. More than 98 earthquakes were recorded and analyzed during this time providing new insights to understand the intraplate seismicity in the NW of Iberia.

This study, independently of its regional significance, provides a case example for the use of low magnitude intraplate seismicity to characterize in 3D structures that remain close to failure. It provides a first image of the Ventaniella Fault and its crustal scale, with earthquakes reaching at least 20 km depth. The results are, to an extent, unexpected because they show a linear pattern that projected to the surface is oblique to the trace of the main fault. Since the majority of the earthquakes are generated at mid crustal depths, other regional factors favouring stress concentration and amplification in the crust around the study area will be explored in the discussion.

TECTONIC SETTING

The present crustal architecture of the NW Iberian Peninsula is a consequence of two orogenies, the Variscan (Late Palaeozoic) and the Alpine (Cenozoic) orogeny, and several rifting episodes in the Mesozoic. A rifting episode in the Permian is relevant to the study area because it generated the NW striking faults, and associated basins (e.g. Martínez-García et al., 2004), and some minor NE faults, that were both later reactivated during the Alpine convergence. The main rifting episode in the Mesozoic resulted in the opening of the Bay of Biscay and the formation of a new plate boundary between Iberia and Europe that was closed later during the Alpine orogeny. Between the Mid Eocene and Early Miocene, the approximate N-S convergence produced the rise of the Cantabrian Mountains, a consequence of the partial underthrusting of the transitional crust formed in the Bay of Biscay underneath the Iberian microplate (Álvarez-Marrón et al., 1997; Fernández-Viejo et al., 1998, 2000; Gallastegui et al., 2002; Pedreira et al., 2003). Within the continental crust, the convergence produced thrusts, strike-slip faulting, retightening of Variscan upright folds, and a general tectonic vergence to the South (Ferrus-Piñol, 1994; Santanach, 1994; Alonso et al., 1996; Martín-González and Heredia, 2011 a,b). Deep geophysical profiling shows an average crustal thickness of 30-32 km to west of the Cantabrian Mountains (Córdoba et al., 1987; Fernández-Viejo et al., 2000; Díaz and Gallart, 2009), while a thickening of the crust up to 50-55 km in its central and eastern zones (Pulgar et al., 1996; Fernández-Viejo et al., 1998; 2000; Pedreira et al., 2003).

The Ventaniella Fault has a surface trace in geological maps that can be followed for more than 400 km crossing the Cantabrian Mountains and continental margin from NW to SE, and affecting Paleozoic and Mesozoic materials (Julivert et al., 1971; Tavani et al., 2011; Viejo et al., 2014) (Figures 1, 2). While the cartographic pattern of the fault is straightforward through the Paleozoic formations, which are steeply dipping, its recognition becomes more challenging through the Mesozoic formations, which are flat lying and not so well exposed. Its origin and particularly its evolution is debated and/or poorly known; there are parts of the fault that reactivate Permian structures, others that reactivate late Variscan structures. Its last amply recognized movement corresponds to an oblique dextral fault with a reverse component, which results in a slight elevation of the NE block (Alonso et al., 1996) (Figure 3). In the area of Peñas cape (Figure 1), the fault elevates 50 meters a sector of the emerged Cantabrian wavecut platform (Díaz-Díaz, 2016). Inland the effect on the topography is very limited, although it is worth noting that determines the orientation of a secondary watershed between the Nalón river and the Infierno and Ponga rivers (Figure 3) (Álvarez-Marrón, 1989).

The trace of the Ventaniella Fault roughly coincides with the western boundary of the aborted rift branch off the Tethys during Permian times that extends from the SE (Arche and López-Gómez, 1996). It has also been proposed that this direction follows an important rift domain boundary from the earliest phases of post-Variscan extension (Cadenas el at., 2017). Subsequent rifting episodes in the Mesozoic do not overprint the Ventaniella itself, but affected the continental crust to the East of this structure (Ziegler, 1988; 1992). During the Alpine convergence, part of the shortening was accommodated by crustal thickening of a previously extended crust forming what it is now the crustal root beneath the Cantabrian Mountain range. The mapped trace of the Ventaniella Fault roughly coincides with the western termination of this Alpine crustal root (Figure 2). Although the depth of the fault and its dip has not been confidently established, it has been assumed to be quasi-vertical (Alonso et al., 1996; García-Mayordomo et al., 2012) and it has been suggested that it could reach the whole crust (Viejo et al., 2014). Its possible role as a structure separating two domains, applies to seismicity (practically absent immediately to the East of the fault) and to images of lithospheric and crustal variations based on seismic refraction data and tomographic studies (Díaz et al., 2016; Palomeras et al., 2017; Villaseñor et al., 2007). However, how the transit between domains takes place is poorly constrained and the inclination at depth of the fault or its possible rooting into the lower crust is enigmatic.

THE VENTANIELLA SEISMIC NETWORK

Between September 2015 and March 2017, a portable seismic network consisting on 10 seismographs was deployed to monitor the 70 km long active segment of the Ventaniella Fault (Figure 3). Eight of the ten stations were situated surrounding the segment and two of them were deployed right on top of the trace of the fault. The minimum interstation distance was 14 km and the maximum reached 51 km, being on average 18 km. The network recorded continuously for 19 months.

The selection of the ten sites considered aspects such as noise levels, communications, geological conditions and/or accessibility. The used data-logger was a 24-bit-SRU-Spider, equipped with GPS antennas and with short-period Geospace MiniSeis-Monitor seismometers with three components. The equipment was powered by solar panels in continuous recording and with a sampling frequency of 100 sps, being operated remotely through a TCP/IP protocol.

Data processing was done with SEISAN software (Havskov and Ottemöller, 1999). The detection of events within the continuous recording was performed through an algorithm STA/LTA (STA length = 0.3 s; LTA length = 60 s; min. trig. duration = 1.5 s; min. trig. interval = 15 s; filter = 2-16 Hz), selecting events that had been registered by at least three of the stations. After identifying the local events of natural origin, the seismic phases were picked manually (see examples in Figure 4).

To locate the hypocenters we have used the HYPOCENTER program (Lienert et al., 1986; Lienert, 1991; Lienert and Havskov, 1995) obtaining in each case their M_L and M_W magnitudes. The velocity model used was a 1d model of seven layers with a Vp/Vs ratio= 1.74, based on earlier studies and crustal structure local models (Figure 5). Focal mechanisms were determined for 16 events which showed clear polarities, using initial motion polarity P waves analyzed with the FPFIT program (Reasenberg and Oppenheimer, 1985). However, in order to verify the stability of the proposed solutions the results were compared with others through the programs FOCMEC (Snoke et al., 1984), HASH (Hardebeck and Shearer, 2002, 2003) and PINV (Suetsugu, 1998).

RESULTS

The total number of events detected through the algorithm used was 6,413, which were analyzed individually. A total of 98 local earthquakes were recovered, the rest being "false triggers" (quarry blasts, teleseismic events, etc.). Figure 4 shows several seismograms recorded by the Ventaniella network illustrating the data quality. Also shown are the picked arrivals with their uncertainty used to perform the study. Within the area of interest, we locate a total number of 45 events with magnitudes $M_W<2$, at depths up to 20 km, although the majority are restricted to the 9-18 km depth range (Figure 3; Table 1). The threshold of detection is estimated as $M_L=0$, and the average error in the epicentral locations < 1.7 km, being the maximum uncertainty in the determination of depth of 2.6 km. The distribution of events in time has been continuous with an average of 2.5 events per month. It is worth to note that during the same period of recording, the national network from IGN only registered 2 of those events of magnitude 1.7 and 2.1 m_bLg, occurred on 3/12/2016 and 12/03/2017 and located at 4 and 3 km from our locations, respectively.

Figure 3 shows that earthquakes are spatially distributed along a linear trend oriented NW-SE within the sector of the fault with previously reported seismicity (Figure 3). Along this alignment, from the SE to the NW there is a progressive separation of the epicenters from the surface trace of the fault towards the West. This oblique arrangement was never clearly observed before with the previous seismic networks, which in general show a higher dispersion of events, both due to the lower resolution and the uncertainty in the location of the national network.

To improve our image of this geometry, we refined the location of the events using the double difference technique (HypoDD; Waldhauser and Ellsworth 2000; Waldhauser 2001). We used the following parameters in the HypoDD program: MAXDIST = 150 km, MAXSEP = 10 km, MAXNGH = 99, MINLNK = 6; MINOBS = 1, MAXOBS: 10. 37 earthquakes from the catalogue elaborated through the portable network could be relocated with this technique. The events trend

N35ºW with a plunge of 19º (Figure 6; Table 2). Moreover, we can distinguish two subgroups, labeled A and B in Figure 6, separated by a gap of about 10 km.

The group A, situated to the NW has 26 earthquakes trending for about 29 km along the NW direction, spreading in width about 5 km. Their depths also increase to the NW, from 11.7 to 21 km. Within this group, 14 focal mechanisms were determined, being predominant the movements with strike slip and reverse fault solutions (Figure 6; Table 3). The group B, to the South, clusters around the vicinity of the Riaño reservoir, is composed by 11 events, dispersed within an area of 14 x 8 km at depths between 7 and 16 km. The only two solutions obtained for group B indicate movements of a normal fault with fault planes oriented E-W. From the image of the distribution at depth of the seismicity showed on Figure 3 it is noticeable that both groups seem to have a different nature, being group A more homogeneous and with a clear trend, while group B shows a diffuse pattern with no clear directional trend in it. This is better defined in Figure 6 where relocated hypocenters are plotted.

DISCUSSION

Interpretation of the seismicity pattern

The Ventaniella Fault presents inland an active segment to the South, being apparently aseismic to the North. The local seismic network deployed for this work shows that, in fact, two groups of earthquakes can be differentiated according to their clustering and distribution: a group A, showing a linear trend slightly oblique to the main trace of the Ventaniella Fault, and a group B, more disperse and with a poorly developed alignment with the Ventaniella Fault.

The simplest geometric arrangement of structures that may explain this seismicity pattern are fault intersections. Fault intersections are characterized by intense fracturing, incrementing the values of permeability and fluid circulation (e.g. Talwani, 1989; Marshak and Paulsen, 1997; Sibson, 1988). The mechanical constrast with respect to stronger neighbouring regions may favour the nucleation of seismicity (Talwani, 1999; Bonini et al., 2016; Aochi and Kato, 2010; Yamini-Fard et al., 2006; Gangopadhyay and Talwani, 2005; Pace et al., 2002; Hildenbrand et al., 2001). In addition to this, deep reaching fault zones are also characterized by a reduced frictional angle (Cloetingh et al., 2005), and therefore they should be prone to reactivation at stress levels well below those required to form new ones.

In the present case, the linear seismicity pattern plunges 19°N, implying that at least one of the intersecting fault must be a low angle structure. This in itself is an unexpected result of this contribution, since to date, no seismicity was associated in the Cantabrian Mountains with low angle faults. There are two possible interpretations involving the intersection of faults that explain the origin of the activity for the group A. The first involves the intersection between a south dipping Ventaniella Fault and the north dipping frontal thrust of the Cantabrian Range. This would require the Ventaniella Fault to dip 76°SW and the frontal thrust of the Cantabrian Mountains to dip around 20°N, the latter in agreement with geological sections in the study area (16-18° in Alonso et al. (1996) and Pulgar et al. (1999)) (Figure 7a). The Ventaniella Fault has been found in outcrops to be subvertical along most of its trace (Álvarez-Marrón, 1989) and in its first 10s of meter. At depth, its dip is less certain but seismic profiles at the submerged continental platform in its northern edge also indicate a subvertical discontinuity within the basement (Viejo et al., 2014). Therefore, its intersection with the low angle dipping thrust of the Cantabrian Mountains would fall within the localized cluster of seismicity. As a counterargument, the cluster may indicate that the Ventaniella Fault is a vertical fault until 20 km depth at least.

The separation of the cluster towards the West from the surface trace of the fault suggests a second viable and alternative geometry. In this case, the responsible structure would be an oblique fault branching off the Ventaniella Fault (Figure 7a), striking N67ºW and dipping 80ºNE, beginning near the Riaño Reservoir, and also intersecting the frontal thrust of the Cantabrian Mountains dipping 20ºN (Figure 7b). This oblique fault has a shorter mapped trace compared with the larger Ventaniella Fault, and for the purpose of this discussion we propose to name it the Tarna Fault, as the only recognized town it crosses is the mountain village of Tarna, which also gives name to a mountain pass nearby. The trace of the fault at the surface is not straightforward as it coincides with a structurally complicated area which follows the trace of the fault.

Both hypotheses can explain geometrically the seismicity pattern for group A. The Tarna branch running N67ºW presents a more favorable orientation to have been reactivated during the Alpine convergence being also coherent with the current state of stress, with the maximum shortening oriented approximately N-S (Lepvrier and Martínez García, 1990; Alonso et al., 1996; Herráiz et al., 2000; Gárate et al., 2015; Llana-Fúnez and López-Fernández 2015). In any case, either the Tarna Fault and or the main Ventaniella Fault, could be considered part of the same fault system as both imply similar kinematics. Current observations highlight the need for additional deep geophysical profiling to elucidate if one or the other are responsible for the clusters, or alternatively, whether they both merge at depth.

The second cluster of earthquakes, group B, is associated to the trace of the Ventaniella Fault but showing bigger dispersion and slightly shallower seismicity. In contrast with cluster A, the cloud of earhquakes (Figure 6) does not require a low dipping fault. There are two major faults in the vicinity of the cluster, the Ventaniella Fault and the León Fault, that runs East-West (Figure 7). The León Fault is a major tectonic structure originated during the Alpine convergence which produced the rise of some sierras in the Cantabrian Mountains (Alonso et al., 1996). It dips 65-70º to the North according to the works of Alonso et al. (1996) and Pulgar et al. (1999), thus it cannot be geometrically responsible for the seismic alignment of group A, however, its role in triggering seismicity cannot be discarded for the southern cluster, group B (Figure 7), in association to the Ventaniella Fault.

The interpretation of focal mechanisms requires some caution considering the low magnitude of the events but generally the solutions are consistent with the geological record: the dominant signal is that of North-South compression direction, accommodated either by E-W thrust planes or by NW-SE strike-slip faults. For the bigger earthquake in the region, 3.7 (m_bLg), the focal solution indicates a dextral movement of the fault. Group B shows dominant normal fault solutions with nodal planes E-W, again supporting the idea that this cluster may relate to the León Fault and not to the Ventaniella Fault (Figures 6, 7).

The regional structure of the crust: the presence of a major gradient in crustal thickness

The tectonic setting for the active fault intersections within the continental crust in the Cantabrian Mountains may also help in the understanding of the underlying processes that produce the accumulation of stresses away from an active plate boundary. The most remarkable feature of the continental crust under the Cantabrian Mountains is the presence of a crustal root, that reaches 45-55 km in thickness in the central part of the orogen (Pulgar et al., 1996; Fernández-Viejo et al., 2000). The thickness of the crust decreases to the West, where normal 32 km thick crust is encountered, therefore implying a very significant lateral gradient in crustal thickness (Figure 2).

Results from deep seismic refraction (Fernández-Viejo et al., 2012; Díaz et al., 2016), and analysis of seismicity by teleseismic and ambient noise analysis (Palomeras et al., 2017; Villaseñor et al., 2017) show that two different crustal/lithospheric blocks exist beneath Galicia and beneath the eastern side of the Cantabrian Mountains. The boundary between them follows approximately a northerly direction and coincides in part, although at an oblique angle, with the trace of the Ventaniella Fault (Fig. 2). The seismically active studied area in this contribution overlaps the strongest lateral gradient in thickness, 15-25 km in vertical in less than 50 km in horizontal.

The tectonic history of the crust on either side of the Ventaniella Fault is also significantly different. Parts of the Ventaniella Fault formed during the Permo-triassic stretching phase after the Variscan orogeny, where extension started to individualize two blocks, a normal crust to the SW and a thinning one to the NE (Cadenas et al., 2017). Subsequent extensional events in the Mesozoic enhanced these early differences to either side of the fault, as extension was preferentially accommodated in the crust to the East of the Ventaniella Fault. During the Alpine convergence, thickening have also preferentially affected portions of the crust that were previously extended, the latter is a general feature of the Cantabrian-Basque-Pyrenees (e.g. Pedreira et al., 2003; Gallastegui et al., 2016; Ruiz et al., 2017).

Sharp gradients in crustal thickness are expected to generate loading stresses in the crust, as reported in other scenarios around the world (Mandal, 2011; Mishra, 2016; Mooney et al., 2012; Tesauro et al., 2015). There are examples of this interaction between deep lateral gradients and appearance of seismicity in the crust, i.e. Mishra (2016), studying seismicity associated to gravity highs in Kachch and Shillong Plateau, refers a coincidence on the location of a Moho ramp between 36 and 56 km depth and the increase of seismicity. Thurber et al. (2009), in a 3D model of the crustal structure in California, found also an increased activity associated to a major lateral velocity contrast and sharp gravity gradient within the transition between the Coast Ranges and the Great Valley. Closer to the study area, in the western Pyrenees, seismicity has been related to high density blocks in the crust sinking even when there is also other high density blocks which do not show seismicity (Souriau et al., 2014).

The role of the lithosphere in the stabilization of isostatic misbalance crustal density inhomogeneities is a spreading idea and vertical motions are argued to explain earthquakes in other intracontinental settings, not only Pyrenees (Dumont et al., 2015), but also in western US (Becker et al., 2015; Levander and Miller, 2012). Nur et al. (1993) proposed that abrupt gradients in Moho and lithospheric thickness were more likely to be zones of deformation than physiographic boundaries. Panza et al. (1980) based on a statistical analysis in seismicity concluded that the aseismic slip below the Moho may be a key seismogenic process, observing a concentration of events in relation to large gradients in lithospheric thickness. Seismicity, then, can cluster in areas of lithospheric strength boundaries arising from changes in crustal thickness or geothermal variations. In the model of Becker et al. (2015), the physical interpretation suggests that intraplate seismicity responds to changes in vertical stress rates being found in areas with elevated gravitational potential energy. Sandiford and Engholm (2008) find a correlation with thermal structuration arising from the differences in crustal thickness across a passive continental margin in Australia to induce seismicity away from the plate boundary. Hence, Moho depth gradients contribute to localization, since they lead to local enhanced strain rates. Cloetingh et al. (2005) further suggest that the location of faulting and seismicity is controlled by abrupt changes in integrated lithospheric strength. In a map of this parameter for western Europe a weak transition is observed between the western and eastern Cantabrian Mountains (Cloetingh et al., 2005). Thomas and Powell (2017) indicate that restricted areas of concentrated crustal deformation along parts of regional basement structures is a necessary condition for intraplate earthquakes. But they also indicate that the clusters are limited to specific segments along the whole length of these structures (such as in Ventaniella Fault) implying that an extra local condition must be present to affect the crustal strength.

Hazard assessment

The current study is based on a limited number of earthquakes of very low magnitude. For this reason, caution is needed when proposing that this particular area poses a real hazard or that it has been will be active for a long period of time. The Alpine convergence, the geodynamic context in which the Ventaniella Fault was mainly developed, terminated in northern Iberia in late Oligocene; however, there is evidence for more recent tectonic activity, for example in the southern segment of the Ventaniella Fault, Nozal and Gracia (1990) recognised offset Pleistocene alluvial deposits, subsequently capped by middle to upper Pleistocene fans. The extent of the tectonic activity during the Quaternary remains to be determined in detail.

Concerning the state of the current stresses in the region the few existing studies, based on the analysis of focal mechanisms and fault distribution patterns, indicate a northwesterly $\sigma_{h\ max}$ at the westernmost end (Herráiz et al., 2000; Andeweg, 2002, De Vicente et al., 2008) adopting a northerly orientation in the Cantabrian Margin (Lepvrier and Martínez-García, 1990). In contrast to the extensive literature on the contact between the Euroasiatic and African plates in Southern Iberia (e.g. Pérez-Peña et al., 2010, Echeverría et al., 2013, Rosado-Moscoso et al., 2017), deformation rates at the northwestern Iberian Peninsula have been scarcely studied. Palano et al. (2014), based on geodetic data (1999-2012), estimate an E-W oriented strain rate contraction up to $1.74 \cdot 10^{-15}$ s^{-1} in the NW of Iberia. Gárate et al. (2015), based on 4-year data from a permanent

GPS network, observe movements at the westernmost end of 1.09 mm/yr in the N13ºW direction, while for the Cantabrian sector they are estimated at 0.29 mm/yr in the N39ºE direction to west of the Ventaniella Fault and 0.96 mm/yr in the N13ºW direction to the East. In that same study, at the Iberian scale, the strain rate field estimated for the northwest region of Iberia result in a dilatation rate $< 10^{-16}$ s^{-1}, while the main horizontal strain rate axes has an approximate N-S orientation.

A major challenge to establish the hazard of this fault are the climatic characteristics of the Cantabrian Mountain range, determined by its latitude, orientation and proximity to the Ocean: any fault offset reaching the surface is rapidly eroded. Landslides are frequent in the Cantabrian Mountains and although large old ones may have been due to earthquakes, most can be attributed to the conjunction of the dynamics of a pluvio temperate climate, argillaceous ground and rough topography (e.g. Domínguez-Cuesta et al., 1999).

A generic approach to evaluate hazard in this particular region within the Iberian Peninsula come from statistic analysis of seismicity record on a much larger region. Likewise, the instrumental catalogue for the study area only includes the last 4 decades. Therefore, it is possible that the long term seismic hazard may not be well captured from this catalogue.

Villamor et al. (2012) in a detailed study on the Alentejo-Plasencia Fault, includes some preliminary anlysis of fault activity in structures in the Cantabrian Mountains. They estimated a net slip rate for the Ventaniella Fault of 0.05 mm/y and (+/- 0.01 error) for a segment of the fault located at the SE of our seismic network, and proposes for this fault a recurrence interval for a maximum magnitude 7 earthquake (with a low reliability) of 30,000 years with an extreme error bar between around 4,600 and almost 60,000 years. This study concluded that the type of active faults such as the Ventaniella Fault do not contribute significantly to seismic hazard in the Iberian Peninsula at the short return periods typical of building codes, ~500 years, and proposes a revision for larger return periods (important for critical constructions such as large dams, nuclear power plants, etc.). More recently, in a study based on a seismic record that spans tens of years and that covered the whole Iberian Peninsula and neighbouring regions, Gaspar-Escribano et al. (2015) estimated in relative terms a very low level of hazard for the study area.

CONCLUDING REMARKS

The deployment of a temporary seismic network between 2015 and 2017 along the seismically active sector of the Ventaniella Fault helped clarify the structures generating the seismicity along parts of this fault. Only with this type of network is possible to obtain locations sufficiently reliable for seismotectonic studies in areas of low magnitude seismicity. The events were grouped in two distinct clusters, A and B, separated by a 10 km gap. The differences in their geometry point to a slightly different origin. A precise hypocentral determination of 37 events through the double difference technique has resulted in the foci aligned along the direction N35ºW and plunging 19ºNW for cluster A. In contrast, cluster B forms a diffuse distribution. The focal mechanism solutions indicate a dominant movement of reverse fault for group A and normal fault with nodal plane E-W for group B. The interpretation on the origin of the seismicity clusters points out to the intersection between the Ventaniella Fault or a secondary branch off the fault (named here the Tarna fault) to the West with the frontal thrust of the Cantabrian Mountains for the group of events A and between the Ventaniella Fault with the E-W León Fault for the group of events B. The most remarkable feature from the data set is that for the first time, the seismicity is associated with a low angle structure, the frontal thrust of the Cantabrian Mountains. The detailed study of the seismicity has proven to be very useful in advancing in the understanding of the internal structure of the crust in the Cantabrian Mountains, and opens up the possibility for future work.

Both clusters of earthquakes studied coincide with the western termination of an Alpine crustal root under the Cantabrian Mountains. The sharp gradient in crustal thickness, from 50 km to 30 km in thickness in less than 50 km horizontal distance, may have been sufficient to increase regional loading stresses bringing some of the crustal-scale structures in the Cantabrian Mountains, such as the Ventaniella Fault system, the León Fault or the frontal thrust of the Cantabrian Mountains, close to failure.

In an area short of data related to strain rates, GPS measurements and other geodetic information, the proposed role of lateral gradients in crustal thickness as a necessary factor to rise regional stresses within the crust needs to be assessed in future works. In stable, intraplate scenarios, away from plate boundaries, stresses are expected to be relatively low. Seismicity on old structures requires mechanisms that either weaken the crust along those structures to allow fault ruptures or, alternatively, mechanisms that amplify stresses at those inherited structures sufficiently to promote movement. In this respect, the results in this contribution bring new lines of work in the Cantabrian Mountains, but also may provide an example for other regions characterized by similar phenomena.

DATA AND RESOURCES

The local seismicity data presented and used in this study were collected using a seismic network funded by projects MISTERIOS and GEOCANTABRICA and can be released to the public on demand at GEOCANTABRICA@ftp.geol.uniovi.es.

The regional seismicity data can be obtained from the Spanish Seismic Network at www.ign.es (last access July 2017).

ACKNOWLEDGEMENTS

CLF, JO and SLF acknowledge financial support to the GEOCANTABRICA research group through a grant (GRUPIN14-044) from the Government of the Principality of Asturias and FEDER funds. The seismicity data was acquired in collaboration with project MISTERIOS (grant CGL2013-48601-C2-2-R) from the Ministry of Economy and Competitiveness of the Government of Spain, who also supported GFV. SLF acknowledges additional funding for the study of the fault rocks along the Ventaniella Fault (grant CGL2014-53388-P). We thank M. Ruiz, J.M. González-Cortina, M.J. Domínguez-Cuesta and J.L. Alonso for their feedback at different stages during the development of this research. We also appreciate the coments of by two reviewers and the BSSA Editor, which have allowed us to substantially improve the article.

REFERENCES

Alonso, J. L., J. A. Pulgar, J. C. García-Ramos, and P. Barba (1996). Tertiary basins and Alpine tectonics in the Cantabrian Mountains, in: *Tertiary Basins of Spain* P. F. Friend and C. J. Dabrio (Editors), Cambridge Univ. Press, Cambridge, U. K., 19-22.

Álvarez-Marrón, J. (1989). *La estructura geológica de la Región del Ponga (Zona Cantábrica, NW de España)*. PhD thesis, Univ. of Oviedo, 1-223.

Álvarez-Marrón, J., E. Rubio, and M. Torné (1997). Subduction related structures in the North Iberian Margin, *J. Geophys. Res.* 102 497-511.

Andeweg, B. (2002). *Cenozoic tectonic evolution of the Iberian Peninsula: Effects and causes of changing stress fields.* Phd thesis, Vrije Universiteit Amsterdam, 1-178.

Aochi, H., and A. Kato (2010). Dynamic rupture of crosscutting faults: a possible rupture process for the, 2007 Mw6.6 Niigata-ken Chuetsu-oki earthquake, *J. Geophys. Res*. 115 B05310.

Arche, A., and J. López-Gómez (1996). Origin of the PermianTriassic Iberian Basin, central-eastern Spain, *Tectonophysics* 266 443-464.

Becker, T. W., A. R. Lowry, C. Faccenna, B. Schmandt, A. Borsa and Q. Yu (2015). Western US intermountain seismicity caused by changes in upper mantle flow, *Nature* 524 458-461.

Bent, A. L. (1994). The 1989 (M s 6.3) Ungava, Quebec, earthquake: a complex intraplate event, *Bull. Seism. Soc. Am.* 84, 1075-1088.

Bollinger, L., M. Nicolas, and S. Marin (2010). Hydrological triggering of the seismicity around a salt diapir in Castellane, France, *Earth Planet. Sci. Lett.* 290 20-29.

Bonini, M., G. Cortia, D. Delle Donneb, F. Sanic, L. Piccardia, G. Vannuccid, R. Gencoc, L. Martellie, and M. Ripepec (2016). Seismic sources and stress transfer interaction among axial normal faults and external thrust fronts in the Northern Apennines (Italy): A working hypothesis based on the 1916-1920 time-space cluster of earthquakes, *Tectonophysics* 680 67-89.

Cadenas, P., G. Fernández-Viejo, and J. A. Pulgar (2017). A Permo-Triassic border rift structure within the south-western Bay of Biscay controlling the shape of the Alpine crustal root beneath the Cantabrian Mountains *Geophys. Res. Abst*. 19 EGU2017-12721.

Calais, E., T. Camelbeeck, S. Stein, M. Liu, and T. J. Craig (2016). A new paradigm for large earthquakes in stable continental plate interiors, *Geophys. Res. Lett.,* 43.

Cloetingh, S., P. A. Ziegler, F. Beekman, P. A. M. Andriessen, L. Matenco, G. Bada, D. García-Castellanos, N. Hardebol, P. Dezes, and D. Sokoutis (2005). Lithopsheric memory, state of stress and rheology: neotectonic controls on Europe´s intraplate continental topography, *Quat. Sci. Rev.* 24 241-304.

Córdoba, D., E. Banda, J. and ansorge (1987). The Hecynian crust in NW Spain, *Tectonophysics* 132 321-333.

Costain, J. K. (2008). Intraplate seismicity, hydro seismicity, and predictions in hindsight, *Seismol. Res. Lett.* 79 579-589.

Costain, J. K., G. A. Bollinger, and J. A. Speer (1987). Hydroseismicity - a hypothesis for the role of water in the generation of intraplate seismicity, *Geology* 15 618-621.

Custodio, S., N. A. Días, F. Carrilho, E. Gongora, I. Rio, C. Marreiros, I. Morais, P. Alves, and L. Matías (2015). Earthquakes in western Iberia: improving the understanding of lithospheric deformation in a slowly deforming region, *Geophys. J. Int.* 203 127-145.

De Vicente, G., S. Cloetingh, A. Muñoz-Martín, A. Olaiz, D. Stich, R. Vegas, J. Galindo-Zaldívar, and J. Fernández-Lozano (2008). Inversion of moment tensor focal mechanisms for active stresses around the microcontinent Iberia: Tectonic implications, *Tectonics* 27 TC1009.

Díaz-Díaz, L. (2016). *Caracterización geológica y geotécnica del subsuelo urbano de Avilés y su entorno*, PhD thesis, Univ. of Oviedo, 1-338.

Díaz, J., and J. Gallart (2009). Crustal structure beneath the Iberian Peninsula and surrounding waters: A new compilation of deep seismic sounding results, *Phys. Earth Planet. In.* 173 181-190.

Díaz, J., J. Gallart, and R. Carbonell (2016). Moho topography beneath the Iberian-Western Mediterranean region mapped from controlled-source and natural seismicity surveys, *Tectonophysics* 692 74-95.

Domínguez-Cuesta, M. J., M. Jiménez-Sánchez, and A. Rodríguez-García (1999). Press archives as temporal records of landslides in the North of Spain: Relationships between rainfall and instability slope events, *Geomorphology* 30 125-132.

Dumont, T., A. Replumaz, S. Rouméjon, A. Briais, A. Rigo, and J. P. Bouillin (2015). Microseismicity of the Bearn Range: reactivation of inversion and collision structures at the northern edge of the Iberian plate. *Tectonics*, 34 934-950.

Echeverría, A., G. Khazaradze, E. Asensio, J. Gárate, J. M. Dávila, and E. Suriñach (2013). Crustal deformation in eastern Betics from CuaTeNeo GPS network, *Tectonophysics* 608 600-612.

Fernández-Viejo, G., J. Gallart, J. A. Pulgar, D. Córdoba, and J. J. Dañobeitia (2000). Seismic signature of Variscan and Alpine tectonics in NW Iberia: Crustal structure of the Cantabrian Mountains and Duero Basin, *J. Geophys. Res*. 105 3001-3018.

Fernández-Viejo, G., J. Gallart, J. A. Pulgar, J. Gallastegui, J. J. Dañobeitia, and D. Córdoba (1998). Crustal transition between continental and oceanic domains along the North Iberian margin from wide angle seismic and gravity data, *Geophys. Res. Lett*. 25 4249-4252.

Fernández-Viejo, G., J. A. Pulgar, J. Gallategui, and L. Quintana (2012). The Fossil Accretionary Wedge of the Bay of Biscay: Critical Wedge Analysis on Depth-Migrated Seismic Sections and Geodynamical Implications, *J. Geol. 120* 315-331.

Ferrus-Piñol, B. (1994). Estructura de la cuenca de As Pontes (A Coruña), *Cuadernos do Laboratorio Xeoloxico de Laxe* 19 73-89.

Gallastegui, J., J. A. Pulgar, and J. Gallart (2002). Initiation of an active margin at the North Iberian continent-ocean transition, *Tectonics* 21 1501-1514.

Gallastegui, J., J. A. Pulgar, and J. Gallart (2016). Alpine tectonic wedging and crustal delamination in the Cantabrian Mountains (NW Spain), *J Geophys Res B Solid Earth Planets* 7 1043-1057.

Gangopadhyay, A., and P. Talwani (2005). Fault intersections and intraplate seismicity in Charleston, South Carolina: insights from a 2-D numerical model, *Curr. Sci.* 88 1609-1616.

Gárate, J., J. Martín-Dávila, G. Khazaradze A. Echeverría, E. Asensio, A. J. Gil, M. C. de Lacy, J. A. Armenteros, M. Ruiz, J. Gallastegui, F. Álvarez-Lobato, C. Ayala, G. Rodríguez-Caderot, J. Galindo-Zaldívar, A. Rimi, and M. Harnafi (2015). Topo-Iberia project: CGPS crustal velocity field in the Iberian Peninsula and Morocco, *GPS Solutions* 19 287-295.

García-Mayordomo, J., J. M., Insua-Arévalo, J. J. Martínez-Díaz, A. Jiménez-Díaz, R. Martín-Banda, S. Marín-Alfajem, J. A. Álvarez-Gómez, M. Rodríguez-Peces, R. Pérez-López, M. A. Rodriguez-Pascua, E. Masana, H. Perea, F. Martín-González, J. Giner-Robles, E. S. Nemser, J. Cabral, and QUAFI Compilers (2012). The Quaternary active Faults database of Iberia (QAFI v.2.0), *Journal of Iberian Geology* 38 285-302.

Gaspar-Escribano, K. M., A. Rivas-Medina, H. Parra, L. Cabañas, B. Benito, S. Ruiz Barajas, S., and J. M. Martínez-Solares (2015). Uncertainty assesssment for the seismic hazard of Spain, *Eng. Geol.* 199 62-73.

González-Casado, J. M., and J. Giner (2000). Relaciones entre fallas y sismicidad en el noroeste peninsular, *Geogaceta* 28 71-74.

Gutiérrez Claverol, M., C. López-Fernández, and J. L. Alonso (2006). Procesos neotectónicos en los depósitos de rasa en la zona de Canero (Occidente de Asturias), *Geogaceta* 40 75-78.

Hardebeck, J. L., and P. M. Shearer (2002). A new method for determining first motion focal mechanisms, *Bull. Seismol. Soc. Am*. 92 2264-2276.

Hardebeck, J. L., and P. M. Shearer (2003). Using S/P Amplitude Ratios to Constrain the Focal Mechanisms of Small Earthquakes, *Bull. Seismol. Soc. Am*. 93 2434-2444.

Havskov, J., and L. Ottemoller (1999). SeisAn Earthquake analysis software, *Geophys. Res. Lett.* 70 532-534.

Herráiz, M., G. De Vicente, R. Lindo-Ñaupari, J. Giner, J. L. Simón, J. M. González-Casado, O. Vadillo, M. A. Rodríguez-Pascua, J. I. Cicuéndez, A. Casas, L. Cabañas, P. Rincón, A. L. Cortés, M. Ramírez, and M. Lucini (2000). The recent (upper Miocene to Quaternary) and present tectonic stress distributions in the Iberian Peninsula, *Tectonics* 19 762-786.

Hildenbrand, T. G., W. D. Stuart, and P. Talwani (2001). Geologic structures related to New Madrid earthquakes near Memphis, Tennessee, based on gravity and magnetic interpretations, *Eng. Geol.* 62 105-121.

Kenner, S., and P. Segall (2000). A mechanical model for intraplate earthquakes; application to the New Madrid seismic zone, *Science* 289 2329-2332.

Johnston, A. C. (1989). The Seismicity of 'Stable Continental Interiors' in *Earthquakes at North-Atlantic Passive Margins: Neotectonics and Postglacial Rebound* S. Gregersen, and P. W. Basham (Editors), Dordrecht, Netherlands, Kluwer Academic Publishers, NATO ASI Series Mathematical and Physical Sciences, 299-327.

Johnston, A. C. (1996). Seismic moment assessment of earthquakes in stable continental regions—III. New Madrid 1811-1812, Charleston 1886 and Lisbon 1755, *Geophys. J. Int.* 126 314-344.

Johnston, A. C., L. R. Kanter, K. J. Coppersmith, and C. A. Cornell (1994). *The earthquakes of stable continental regions*, Electric Power Research Institute (EPRI), Palo Alto, 1-309.

Julivert, M., J. Ramírez del Pozo, and J. Truyols (1971). *Histoire Structurale Du Golfe De Gascogne*, Technip, París.

Lepvrier, C., and E. Martínez-García (1990). Fault development and stress evolution of the post-Hercynian Asturias Basin (Asturias and Cantabria, northwestern Spain), *Tectonophysics* 184 345-356.

Levander, A., and M. S. Miller (2012). Evolutionary aspects of lithosphere discontinuity structure in the western U.S. Geochem, *Geophys. Geosys*. 13 Q0AK07.

Lienert, B. R. E. (1991). *Report on modifications made to Hypocenter*, Technical report, Institute of Solid Earth Physics, University of Bergen, Bergen, Norway.

Lienert, B. R. E., E. Berg, and L. N. Frazer (1986). HYPOCENTER: An earthquake location method using centered, scaled, and adaptively damped least squares, *Bull. Seismol. Soc. Am.* 76, 771-783.

Lienert, B. R. E., and J. Havskov (1995). A computer program for locating earthquakes both locally and globally, *Seismol. Res. Lett.* 66 26-36.

Liu, L., and M. D. Zoback (1997). Lithospheric strength and intraplate seismicity in the New Madrid seismic zone, *Tectonics* 16 585-595.

Llana-Fúnez, S., and C. López-Fernández (2015). The seismogenic zone of the continental crust in Northwest Iberia and its relation to crustal structure, *Tectonics* 34 1751-1767.

López-Fernández, C., J. A. Pulgar, J. Díaz, J. Gallart, J.M. González-Cortina, and M. Ruiz (2012) Seismotectonic characterization of the Becerreá area (NW Spain), *Geologica Acta* 10 71-80.

López-Fernández, C., J. A. Pulgar, J. Gallart, J. M. González-Cortina, J. Díaz, and M. Ruiz (2004). Actividad sísmica en el Noroeste de la Península Ibérica observada por la red sísmica local del Proyecto GASPI (1999-2002). *Trabajos de Geología* 24 91-106.

Mandal, P. (2011). Crustal and lithospheric thinning beneath the seismogenic Kachchh rift zone, Gujarat (India): Its implications toward the generation of the 2001 Bhuj earthquake sequence, *Asian J. Earth Sci.* 40 150-161.

Marshak, S., and T. Paulsen (1997). Structural style, regional distribution, and seismic implications of Midcontinent fault-and-fold zones, United States, *Seismol. Res. Lett.* 68 511-520.

Martín-González, F., L. Antón, J. M. Insua, G. de Vicente, J. J. Martínez-Díaz, A. Muñoz-Martín, N. Heredia, and A. Olaiz (2012). Seismicity and potencially active faults in the Northwest and Central-West Iberian Peninsula, *J. Iber. Geol.* 38 31-51.

Martín-González, F., and N. Heredia (2011a). Geometry, structures and evolution of the western termination of the Alpine-Pyrenean Orogen reliefs (NW Iberian Peninsula). *Journal of Iberian Geology* 37 103-120.

Martín-González, F., and N. Heredia (2011b). Complex tectonic and tectonostratigraphic evolution of an Alpine foreland basin: The western Duero Basin and the related Tertiary depressions of the NW Iberian Peninsula, *Tectonophysics* 502 75-89.

Martínez-Díaz, J. J., R. Capote, M. Tsige, P. Villamallor, F. Martín-González, J. M. Arévalo (2006). Seismic triggering in a stable continental area: The Lugo 1995-1997 seismic sequences (NW Spain), *J. Geod.* 41 440-449.

Martínez-García, E., J. F. Antona, A. García-Sánchez, and J. L. Quiroga de la Vega (2004). Tectonic and Metallogenic Significance of Sedimentary Manganese Deposits in the Eastern Cantabrian Domain, Asturias, Northwestern Spain, *Int. Geol. Rev.* 46 273-288.

Martínez-Solares J. M., and J. Mezcua (2002). *Catálogo sísmico de la Península Ibérica (880 a.C.-1990)*, Instituto Geográfico Nacional, Madrid, 1-254.

Mezcua, J., J. Rueda, R. M. García-Blanco (2011). A new probabilistic seismic hazard study of Spain. *Nat. Hazards* 2 1087-1108.

Mishra, D. C. (2016). Seismicity of Kachchh and Shillong Plateau and their connectivity to plate margins. *Journal of Seismology* 20 265-275.

Mishra, O.P., A.P. Singh, D. Kumar, and B.K. Rastogi (2014). An insight into crack density, saturation rate, and porosity model of the 2001 Bhuj earthquake in the stable continental region of western India, *Asian J. Earth Sci.* 83 48-59.

Mooney, W. D., J. Ritsema, and Y. K. Hwang (2012). Crustal seismicity and the earthquake catalog maximum moment magnitude (M-cmax) in stable continental regions (SCRs): Correlation with the seismic velocity of the lithosphere. *Earth Planet. Sci. Lett.* 357 78-83.

Nozal, F., and Gracia, F.J. (1990). El piedemonte de la Sierra del Brezo (Montes Palentinos), in *Actas 1 Reunion Nacional de Geomorfología* M. Gutiérrez-Elorza, and José Luis Peña- Monné (Editors), Proc. I Reunion Nacional de Geomorfología, Teruel, 763-772.

Nur, A., H. Ron, and G. C. Beroza (1993). The Nature of the Landers-Mojave Earthquake Line. *Science*, 261 201.

Pace, B., P. Boncio, G. Lavecchia (2002). The 1984 Abruzzo earthquake (Italy): an example of seismogenic process controlled by interaction between differently oriented sinkinematic faults, *Tectonophysics* 350 237-254.

Palano M., P. J. González, and J. Fernández (2014). An Update GPS Velocity and Strain Rate Fields for the Iberian Region in *Mathematics of Planet Earth* E. Pardo-Igúzquiza, C. Guardiola-Albert, J. Heredia, L. Moreno-Merino, J. Durán , and J. Vargas-Guzmán J. (Editors), Berlin, Springer, 369-372.

Palomeras, I., A. Villaseñor, S. Thurner, A. Levander, J. Gallart, and M. Harnafi (2017), Lithospheric structure of Iberia and Morocco using finite-frequency Rayleigh wave tomography from earthquakes and seismic ambient noise, Geochem. *Geophys. Geosyst.* 18 1824-1840.

Panza, G. F., S. Mueller, and G. Calcagnile (1980). The gross features of the lithosphere-asthenosphere system in Europe from seismic surface waves and body waves, *Pure Appl. Geophys.* 118 1209-1213.

Pedreira, D., J. A. Pulgar, J. Gallart, and J. Díaz (2003). Seismic evidence of Alpine crustal thickening and wedging from the western Pyrenees to the Cantabrian Mountains (North Iberia), *J. Geophys. Res.* 108, B4.

Pérez-Peña, A., J. Martín-Dávila, J. Gárate, M. Berrocoso, and E. Buforn (2010). Velocity field an tectonic strain in Southern Spain and surroundings areas derived from GPS episodic measurments, *J Geodyn* 49 232-240.

Pulgar, J. A., J. L. Alonso, R. G. Espina, and J. A. Marín (1999). La deformación alpina en el basamento varisco de la Zona Cantábrica, *Trabajos de Geología* 21 283-294.

Pulgar, J. A., J. Gallart, G. Fernández-Viejo, A. Pérez-Estaún, J. Álvarez-Marrón, and ESCIN Group (1996). Seismic image of the Cantabrian Mountains in the western extension of the Pyrenees from integrated ESCIN reflection and refraction data, *Tectonophysics* 264 1-19.

Qingsong, L., M. Liu, Q. Zhang, and E. Sandvol (2007). Stress evolution and seismicity in the central-eastern United States: Insights from geodynamic modeling, *Spec. Pap. Geol. Soc. Am.* 425 149-166.

Reasenberg, P., and D. Oppenheimer (1985). *Fpfit, fpplot, and fppage: Fortran computer programs for calculating and displaying earthquake fault plane solutions*, Tech. Rep. U. S. Geol. Surv.

Rosado-Moscoso, B., A. Fernández-Ros, A. Jiménez-Jiménez, and M. Berrocoso-Domínguez (2017). Modelo de deformación horizontal GPS de la región sur de la Península Ibérica y norte de África (SPINA), *Boletín Geológico y Minero*, 128 141-156.

Ruiz, M., J. Díaz, D. Pedreira, J. Gallart, and J. A. Pulgar (2017). Crustal structure of the North Iberian continental margin from seismic refraction/wide-angle reflection profiles, *Tectonophysics* 717 65-82.

Sandiford, M., and D. L. Egholm (2008). Enhanced intraplate seismicity along continental margins: some causes and consequences, *Tectonophysics* 457 197-208.

Santanach, P. (1994). Las cuencas terciarias gallegas en la terminación occidental de los relieves Pirenaicos, *Cuadernos do Laboratorio Xeolóxico de Laxe* 19 57-71.

Satyabala, S. P. (2006). Coseismic ground deformation due to an intraplate earthquake using synthetic aperture radar interferometry: The Mw6.1 Killari, India, earthquake of 29 September 1993, *J. Geophys. Res.* 111.

Schulte, S. M., and W. D. Mooney (2005). An updated global earthquake catalogue for stable continental regions: reassessing the correlation with ancient rifts. *Geophys. J. Int.* 161 707-721.

Sibson, R. H. (1988). Earthquake faulting, induced fluid flow, and fault-hosted gold-quartz mineralization, in *Basement Tectonics: Characterization and Comparison of Ancient and Mesozoic Continental Margins* M. J. Bartholomew, D. W. Hyndman, D. W. Mogk, and R. Mason (Editors), Proc. 8th Int. Conf. Basement, Tectonics, Butte, MT, 603-614.

Snoke, J. A., J. W. Munsey, A. C. Teague, and G. A. Bollinger (1984). A program for focal mechanism determination by combined use of polarity and SV-P amplitude ratio data, *Earthquake Notes* 55 3 15.

Souriau, A., A. Rigo, M. Sylvander, S. Benahmed, and F. Grimaud (2014). Seismicity in central-western Pyrenees (France): A consequence of the subsidence of dense exhumed bodies. *Tectonophysics* 621 123-131.

Stein, S., and Liu, M. (2009). Long aftershock sequences within continents and implications for earthquake hazard assessment. *Nature* 462 87-89.

Suetsugu, D. (1998). *Practice on source mechanism, iisee lecture note*, Technical report, Tsukuba, Japan.

Talwani, P. (1989). Seismotectonics in the southeastern United States in *Earthquakes at North-Atlantic Passive Margins: Neotectonics and Postglacial Rebound* S. Gregersen, and P. W. Basham (Editors), Dordrecht, Netherlands, Kluwer Academic Publishers, NATO ASI Series Mathematical and Physical Sciences, 371-392.

Talwani, P. (1999). Fault geometry and earthquakes in continental interiors, *Tectonophysics* 305 371-379.

Tavani, S., A. Quintà, and P. Granado (2011). Cenozoic right-lateral wrench tectonics in the Western Pyrenees (Spain): The Ubierna Fault System, *Tectonophysics* 509 238-253.

Tesauro, M., M. K. Kaban, and D. W. Mooney (2015). Variations of the lithospheric strength and elastic thickness in North America, *G-cubed* 7 2197-2220.

Thurber, C., H. Zhang, T. Brocher, and V. Langenheim (2009). Regional three dimensional seismic velocity model of the crust and uppermost mantle of northern California. *J. Geophys. Res*. 114 B01304.

Thomas, W. A., and Powell, C. A. (2017). Necessary conditions for intraplate seismic zones in North America. *Tectonics* 36.

Viejo, G., C. López-Fernández, M. J. Domínguez-Cuesta, and P. Cadenas (2014). How much confidence can be conferred on tectonic maps of continental shelves? The Cantabrian-Fault case, *Sci. Rep.* 4 3661.

Villamor, P., R. Capote, M. W. Stirling, M. Tsige, K. R. Berryman, J. J. Martínez-Díaz, and F. Martín-González (2012). Contribution of active faults in the intraplate area of Iberia to seismic hazard: The Alentejo-Plasencia Fault, *Journal of Iberian Geology* 38 85-111.

Villaseñor, A., Y. Yang, M. H. Ritzwoller, and J. Gallart (2007). Ambient noise surface wave tomography of the Iberian Peninsula: Implications for shallow seismic structure, *Geophys. Res. Lett.* 34 L11304.

Waldhauser, F. (2001). HypoDD: A computer program to compute double-difference earthquake locations, USGS Open File Report, 01-113.

Waldhauser, F., and W. L. Ellsworth (2000). A double-difference earthquake location algorithm: Method and application to the northern Hayward fault, *Bull. Seismol. Soc. Am*. 90 1353-1368.

Wolf, L. W., C. A., Rowe, and R. B. Horner (1997). Periodic seismicity near Mt. Ogden on the Alaska British Columbia border: A case for hydrologically triggered earthquakes? *Bull. Seismol. Soc. Am.* 87 1473-1483.

Yamini-Fard, F., D. Hatzfeld, M. Tatar, and M. Mokhtari (2006). Microearthquake seismicity at the intersection between the Kazerun fault and the Main Recent Fault (Zagros, Iran), *Geophys. J. Int.* 166 186-196.

Ziegler, P. A. (1988). *Evolution of the Artic-North Atlantic and the Western Tethys*, American Association of Petroleum Geologists memoir, 43.

Ziegler, P. A. (1992). European Cenozoic Rift system, *Tectonophysics* 208 91-111.

FULL MAILING ADDRESS FOR EACH AUTHOR

López Fernández, Carlos. Department of Geology, C/ Arias de Velasco s/n, 33.005 Oviedo (Spain). Phone: +34 985103110. E-mail: lopezcarlos@uniovi.es

Fernández-Viejo, Gabriela. Department of Geology, C/ Arias de Velasco s/n, 33.005 Oviedo (Spain). Phone: +34 985102932. E-mail: gaby@geol.univoi.es

Olona, Javier. Department of Geology, C/ Arias de Velasco s/n, 33.005 Oviedo (Spain). Phone: +34 985103110. E-mail: olona@geol.uniovi.es

Llana-Fúnez, Sergio. Department of Geology, C/ Arias de Velasco s/n, 33.005 Oviedo (Spain). Phone: +34 985103142. E-mail: llanasergio@uniovi.es

TABLES

Table 1. Hypocenter parameters of the events located in the study area between October 2015 and March 2017. NS = number of stations used for each focal solution; P/S-A = P and S wave arrivals used for each focal solution; MD = minimum distance to the closest station; ERLN, ERLT, ERDP = maximum error in longitude, latitude and depth, respectively.

DATE	HOUR	LAT. (ºN)	LONG. (ºW)	DEPTH (km)	RMS	GAP	N_S	P/S-A	MD (km)	ERLN (km)	ERLT (km)	ERDP (km)	M_L	M_W
02/10/2015	0:08:43	43,045	-5,271	6,7	0,10	105	6	6/6	10	1,0	0,8	3,3	0,6	0,7
19/10/2015	21:35:20	43,150	-5,245	12,8	0,19	108	5	5/5	1	3,0	3,0	2,9	0,2	-
10/01/2016	9:07:04	43,031	-4,983	12,1	0,09	144	8	7/7	8	1,1	0,9	1,8	1,0	1,2
12/01/2016	23:27:18	43,192	-5,010	10,6	0,13	191	3	3/3	7	10,7	6,4	7,6	0,2	-
15/01/2016	3:46:52	43,244	-5,465	16,7	0,11	236	7	5/7	9	2,6	1,6	1,8	0,5	1,1
18/01/2016	0:21:57	42,940	-4,935	9,0	0,10	229	10	10/8	13	1,5	1,0	2,7	1,2	1,4
27/01/2016	7:17:25	43,111	-5,260	14,7	0,07	109	7	6/7	5	1,7	1,0	1,8	0,7	1,1
18/02/2016	11:37:36	43,113	-5,234	12,5	0,13	52	10	10/10	5	0,9	0,8	1,9	0,8	1,3
20/02/2016	19:20:39	43,241	-5,465	20,6	0,13	233	7	7/7	9	3,2	1,4	2,0	0,7	1,3
25/02/2016	19:01:42	43,063	-4,908	8,9	0,13	155	10	10/10	5	1,4	0,8	1,8	0,8	1,2
12/03/2016	7:19:44	43,040	-5,047	2,8	0,10	124	8	8/8	3	1,1	0,8	1,4	0,3	0,4
21/03/2016	1:56:08	42,964	-5,017	10,3	0,13	185	8	7/6	8	1,6	1,5	2,8	0,2	0,7
25/03/2016	3:23:16	43,206	-5,400	18,4	0,18	174	10	10/10	5	2,1	1,5	2,4	1,9	2,0
05/06/2016	8:49:11	43,121	-5,253	12,2	0,12	93	7	7/7	4	1,6	0,9	2,4	0,6	1,0
30/06/2016	9:37:24	43,123	-5,243	12,5	0,17	74	9	9/9	4	1,3	1,0	2,5	1,0	1,2
20/07/2016	3:02:49	43,026	-5,038	1,3	0,19	134	7	7/7	3	1,4	1,1	5,3	0,2	0,7
20/07/2016	3:15:32	42,977	-4,912	11,3	0,13	216	7	7/7	9	2,3	1,7	2,7	0,1	0,9
03/08/2016	7:28:56	42,982	-4,945	14,2	0,10	197	6	5/6	10	2,1	1,9	2,7	0,1	0,8
07/08/2016	19:56:17	43,157	-5,185	16,3	0,16	104	9	8/8	7	1,8	1,2	2,8	0,4	1,0
17/08/2016	17:41:25	43,143	-5,297	12,6	0,10	77	8	8/6	4	1,4	1,0	2,3	0,3	0,7
26/08/2016	0:44:40	43,115	-5,263	13,2	0,15	51	10	9/10	5	1,1	0,9	2,3	0,4	0,9
30/08/2016	1:36:44	43,033	-5,344	9,1	0,12	142	6	6/6	12	2,1	1,2	4,0	-0,2	
02/09/2016	21:34:14	43,158	-5,339	17,7	0,12	79	9	9/9	5	1,6	1,0	2,1	0,8	1,2
27/09/2016	4:58:30	43,132	-5,300	14,2	0,13	63	8	8/8	5	1,6	0,9	2,3	0,6	1,0
10/10/2016	23:17:30	42,976	-4,909	11,1	0,12	218	10	8/9	9	1,6	1,2	2,4	0,8	1,1
16/10/2016	18:03:32	42,986	-4,975	6,8	0,05	182	6	5/5	9	1,3	1,1	2,1	0,2	0,7
29/10/2016	22:58:25	43,144	-5,308	12,7	0,12	67	9	7/8	5	1,5	1,0	2,8	0,3	0,7
30/10/2016	14:07:09	43,135	-5,275	13,2	0,15	66	10	9/9	3	1,4	0,9	1,8	0,6	1,2
13/11/2016	6:35:21	43,042	-4,987	14,1	0,10	245	8	6/7	8	2,4	1,1	2,2	0,5	1,0
03/12/2016	11:12:48	43,096	-5,173	11,2	0,12	91	9	8/8	9	1,1	0,8	2,6	1,5	1,7
10/12/2016	11:40:44	43,040	-5,055	6,8	0,08	223	5	4/3	3	6,5	1,4	2,3	0,1	0,5
16/12/2016	20:54:40	42,953	-4,930	7,5	0,11	223	10	10/9	12	1,6	1,2	3,1	0,8	1,2

30/12/2016	20:55:01	42,979	-5,019	10,6	0,09	174	6	5/5	7	1,6	1,5	3,3	0,0	0,7
08/01/2017	12:22:27	43,030	-5,316	11,1	0,15	92	10	10/9	7	1,5	1,0	2,9	1,3	1,5
14/01/2017	5:46:42	43,172	-5,408	15,4	0,10	215	5	5/5	2	4,2	1,6	3,2	0,4	-
15/01/2017	16:33:34	43,105	-5,210	14,0	0,14	161	6	5/6	6	1,9	1,9	2,8	0,6	1,1
28/01/2017	3:34:02	43,204	-5,434	18,1	0,12	196	10	10/9	6	2,0	1,2	1,9	1,1	1,2
28/01/2017	12:05:10	43,204	-5,425	17,6	0,10	224	8	8/7	5	2,9	1,2	2,0	0,7	1,4
06/02/2017	0:18:47	43,116	-5,247	13,4	0,06	95	7	5/7	4	1,9	0,9	2,5	0,1	-
11/02/2017	6:03:11	43,121	-5,287	16,0	0,11	106	9	9/9	5	1,4	1,0	2,1	0,9	1,0
19/02/2017	21:21:08	43,120	-5,286	16,4	0,10	105	8	8/8	5	1,6	1,0	2,2	0,3	0,7
02/03/2017	5:06:05	43,136	-5,293	14,7	0,14	128	6	5/6	4	2,3	1,6	3,1	0,2	0,6
04/03/2017	18:00:27	43,135	-5,296	14,5	0,11	162	6	6/6	5	1,8	1,5	2,5	0,6	0,9
12/03/2017	9:18:46	43,138	-5,313	15,1	0,04	133	6	5/5	7	1,8	1,2	3,1	1,7	1,6
16/03/2017	0:43:14	43,145	-5,356	17,9	0,10	149	5	3/4	4	2,9	1,9	4,3	0,3	-

Table 2. Hypocenter parameters of the events relocated through the double difference technique (HypoDD).

DATE	HOUR	LAT. (ºN)	LONG. (ºW)	DEPTH (km)
19/10/2015	21:35:19	43,1448	-5,2740	12,2
10/01/2016	9:07:05	43,0295	-4,9864	12,6
15/01/2016	3:46:51	43,2541	-5,4830	16,7
18/01/2016	0:21:58	42,9454	-4,9359	10,9
27/01/2016	7:17:24	43,1207	-5,2827	14,7
18/02/2016	11:37:35	43,1187	-5,2551	12,5
20/02/2016	19:20:37	43,2574	-5,4859	21,0
21/03/2016	1:56:08	42,9636	-5,0108	10,4
25/03/2016	3:23:15	43,2229	-5,4294	17,9
05/06/2016	8:49:10	43,1294	-5,2751	12,1
30/06/2016	9:37:23	43,1283	-5,2587	12,0
20/07/2016	3:15:33	42,9675	-4,9059	12,9
03/08/2016	7:28:56	42,9775	-4,9448	15,9
17/08/2016	17:41:24	43,1529	-5,3132	12,6
26/08/2016	0:44:39	43,1276	-5,2828	12,8
02/09/2016	21:34:13	43,1677	-5,3675	16,5
27/09/2016	4:58:29	43,1420	-5,3226	14,1
10/10/2016	23:17:31	42,9769	-4,9124	12,3
16/10/2016	18:03:33	42,9868	-4,9738	7,1
29/10/2016	22:58:24	43,1550	-5,3283	12,2

30/10/2016	14:07:08	43,1468	-5,3015	11,8
13/11/2016	6:35:21	43,0424	-4,9846	15,7
03/12/2016	11:12:48	43,1005	-5,2024	11,9
10/12/2016	11:40:45	43,0435	-5,0498	7,6
16/12/2016	20:54:41	42,9579	-4,9345	8,2
30/12/2016	20:55:02	42,9791	-5,0202	11,5
14/01/2017	5:46:41	43,1683	-5,4305	16,5
15/01/2017	16:33:33	43,1136	-5,2364	13,9
28/01/2017	3:34:01	43,2148	-5,4548	16,6
28/01/2017	12:05:09	43,2156	-5,4554	16,6
06/02/2017	0:18:46	43,1219	-5,2644	13,7
11/02/2017	6:03:10	43,1268	-5,3095	15,2
19/02/2017	21:21:07	43,1260	-5,3096	15,5
02/03/2017	5:06:04	43,1419	-5,3107	13,5
04/03/2017	18:00:27	43,1449	-5,3179	13,6
12/03/2017	9:18:45	43,1440	-5,3339	15,7
16/03/2017	0:43:13	43,1497	-5,3797	17,7

Table 3. Location and source parameters of the events for which focal mechanisms were determined. PR = number of polarity readings.

N	GROUP	DATE	HOUR	LAT. (ºN)	LONG. (ºW)	DEPTH (km)	MW	PR	STRIKE1	DIP1	RAKE1	STRIKE2	DIP2	RAKE2
1	B	18/01/2016	0:21:57	42,9454	-4,9359	10,9	1,4	5	67	48	79	263	43	-78
2	A	27/01/2016	7:17:25	43,1207	-5,2827	14,7	1,1	6	10	18	78	202	72	94
3	A	18/02/2016	11:37:36	43,1187	-5,2551	12,5	1,3	10	91	58	93	265	32	85
4	A	20/02/2016	19:20:39	43,2574	-5,4859	21,0	1,3	5	35	57	72	246	37	-65
5	A	25/03/2016	3:23:16	43,2229	-5,4294	17,9	2,0	9	135	40	98	305	50	83
6	A	05/06/2016	8:49:11	43,1294	-5,2751	12,1	1,0	7	57	64	39	307	56	-32
7	A	30/06/2016	9:37:24	43,1283	-5,2587	12,0	1,2	7	68	48	-153	319	70	135
8	A	26/08/2016	0:44:40	43,1276	-5,2828	12,8	0,9	9	68	79	139	167	50	-166
9	A	02/09/2016	21:34:14	43,1677	-5,3675	16,5	1,2	8	68	52	-43	188	57	47
10	A	27/09/2016	4:58:30	43,1420	-5,3226	14,1	1,0	8	85	57	-141	331	58	140
11	A	30/10/2016	14:07:09	43,1468	-5,3015	11,8	1,2	7	137	57	138	253	56	41
12	A	03/12/2016	11:12:48	43,1005	-5,2024	11,9	1,7	8	130	40	98	300	50	83
13	B	16/12/2016	20:54:40	42,9579	-4,9345	8,2	1,2	7	70	38	-81	239	52	83
14	A	28/01/2017	3:34:02	43,2148	-5,4548	16,6	1,2	8	88	77	-1	178	89	13
15	A	28/01/2017	12:05:10	43,2156	-5,4554	16,6	1,4	8	42	18	-28	159	82	74
16	A	11/02/2017	6:03:11	43,1268	-5,3095	15,2	1,0	8	132	39	158	239	76	53

LIST OF FIGURE CAPTIONS

Figure 1. Seismic activity in the Cantabrian Mountains and neighbouring areas in the 1980-2017 period and its comparison with the seismicity in Iberia and surrounding regions (inset). The dashed red square indicates the studied area using the portable seismic network. Seismicity data: Spanish Seismic Network (see Data and Resources Section) and GASPI Project (López Fernández et al., 2004).

Figure 2. Moho depth map for the northern half of the Iberian Peninsula from the joint interpolation of DSS and RF estimations, completed with the CRUST1.0 model in the areas not sampled by seismic experiments (From Díaz et al., 2016). Overprinted are: the traces of the Ventaniella Fault (VF), the León Fault (LF) and the frontal thrust of the Cantabrian Mountains. Roughly coincident with the western termination of the crustal root is the trace of the VF.

Figure 3. Map showing the location of the stations belonging to the portable seismic network of Ventaniella (black stars). Also represented are the dots indicating previous instrumental seismicity (empty circles) and activity registered by the network (solid circles). The focal mechanism shown in the figure corresponds to the largest earthquake registered (20/02/1989, mbLg 3.7, Herráiz et al., 2000). In the lower part the projection of the events, there is a longitudinal profile along the fault (represented by three dashed red boxes on the map) and three cross sections to the fault (NW, central and SE).

Figure 4. (a) Example of a seismogram recorded at the CALE station. (b) Image of the vertical canals at all stations during the largest earthquake recorded by the network (03/25/2016; Mw=2.0) in the vicinity of the Ventaniella Fault; first P and S waves have been identified on the seismograms. (c) Characteristic signal produced by a quarry blast registered at the CREM Station on 12/18/2015 with epicenter at 16 km. (d) Record of the same event seen in 8 stations.

Figure 5. 1D velocity model used for the hypocentral determinations, based on Vp velocities obtained in refraction profiles through the study area by Fernández-Viejo et al. (2000).

Figure 6. Map showing the distribution of seismic events after relocation with the double difference technique. 16 focal mechanisms obtained for selected events (see text) are also shown. The focal parameters for the 16 events are listed in Table 3. In the lower part, the projection of the earthquakes in a longitudinal profile to the fault and the cross sections to the fault for A and B subgroups are shown.

Figure 7. 3D Block diagrams illustrating the fault intersections proposed in the text to explain the seismicity recorded. The width of the fault zones is not truly represented, the faults are drawed as simple two dimensional planes. Events located in the "visible side" of the plane are in bright red, events in the "non visible" side in darker red. a) Diagram that shows the intersection between the Ventaniella Fault plane (solid brown) and the frontal thrust of the Cantabrian Mountains (translucid light blue), considering dips of 76˚SW and 20˚N respectively looking from the West and from the Southwest. (b) Sketch showing the intersection between the Tarna Fault (translucid yellow) and the León Fault plane (in dark green), the frontal thrust is shown for reference in translucid light blue.

FIGURES

789

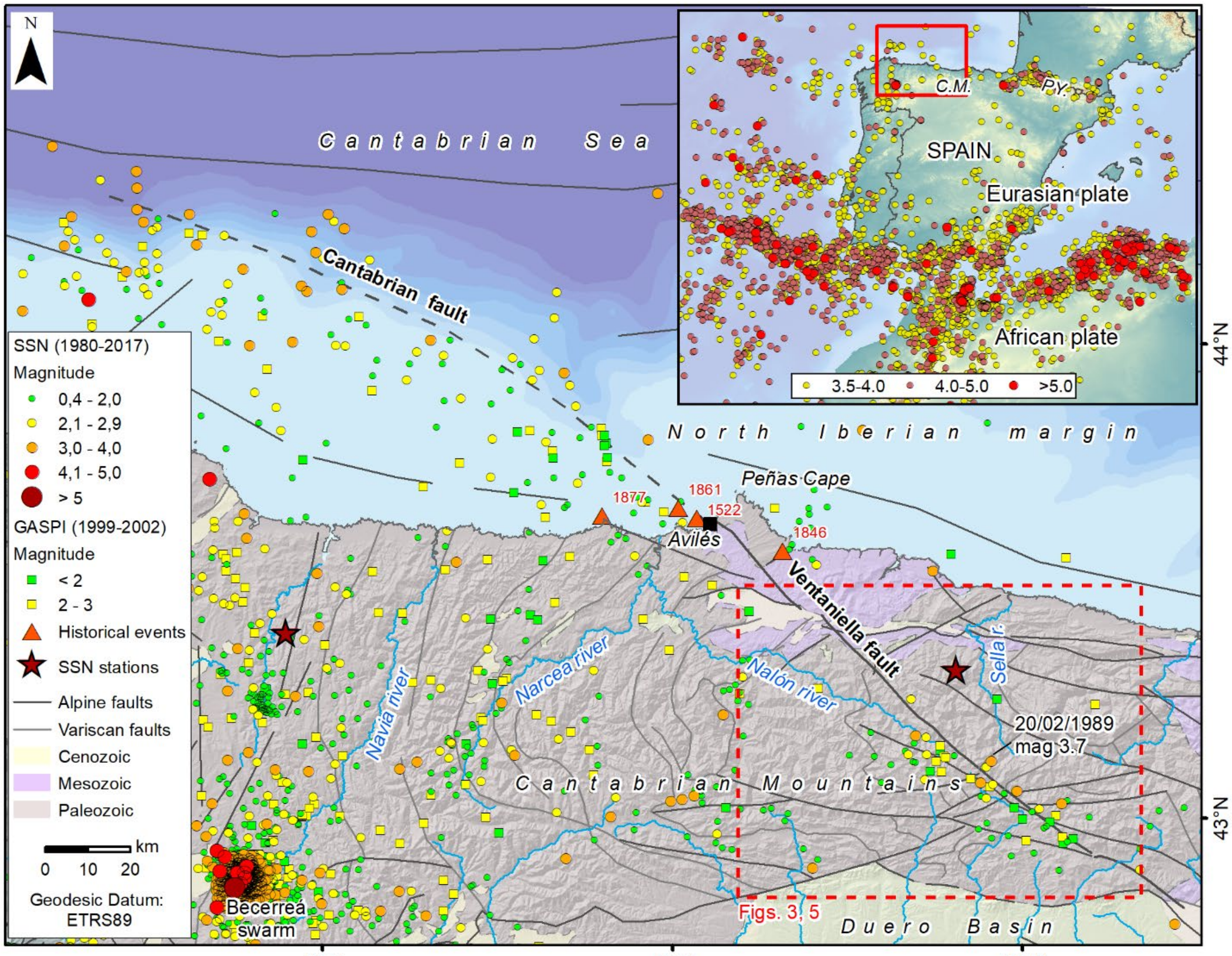

790 Figure 1. Seismic activity in the Cantabrian Mountains and neighbouring areas in the 1980-2017
791 period and its comparison with the seismicity in Iberia and surrounding regions (inset). The dashed
792 red square indicates the studied area using the portable seismic network. Seismicity data: Spanish
793 Seismic Network (see Data and Resources Section) and GASPI Project (López Fernández et al.,
794 2004).

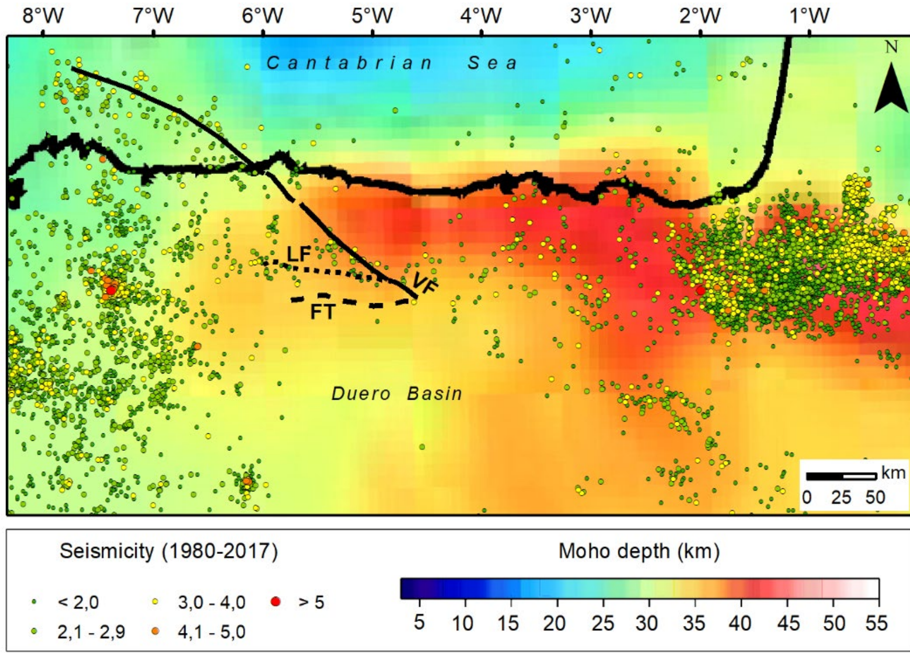

Figure 2. Moho depth map for the northern half of the Iberian Peninsula from the joint interpolation of DSS and RF estimations, completed with the CRUST1.0 model in the areas not sampled by seismic experiments (From Díaz et al., 2016). Overprinted are: the traces of the Ventaniella Fault (VF), the León Fault (LF) and the frontal thrust of the Cantabrian Mountains. Roughly coincident with the western termination of the crustal root is the trace of the VF.

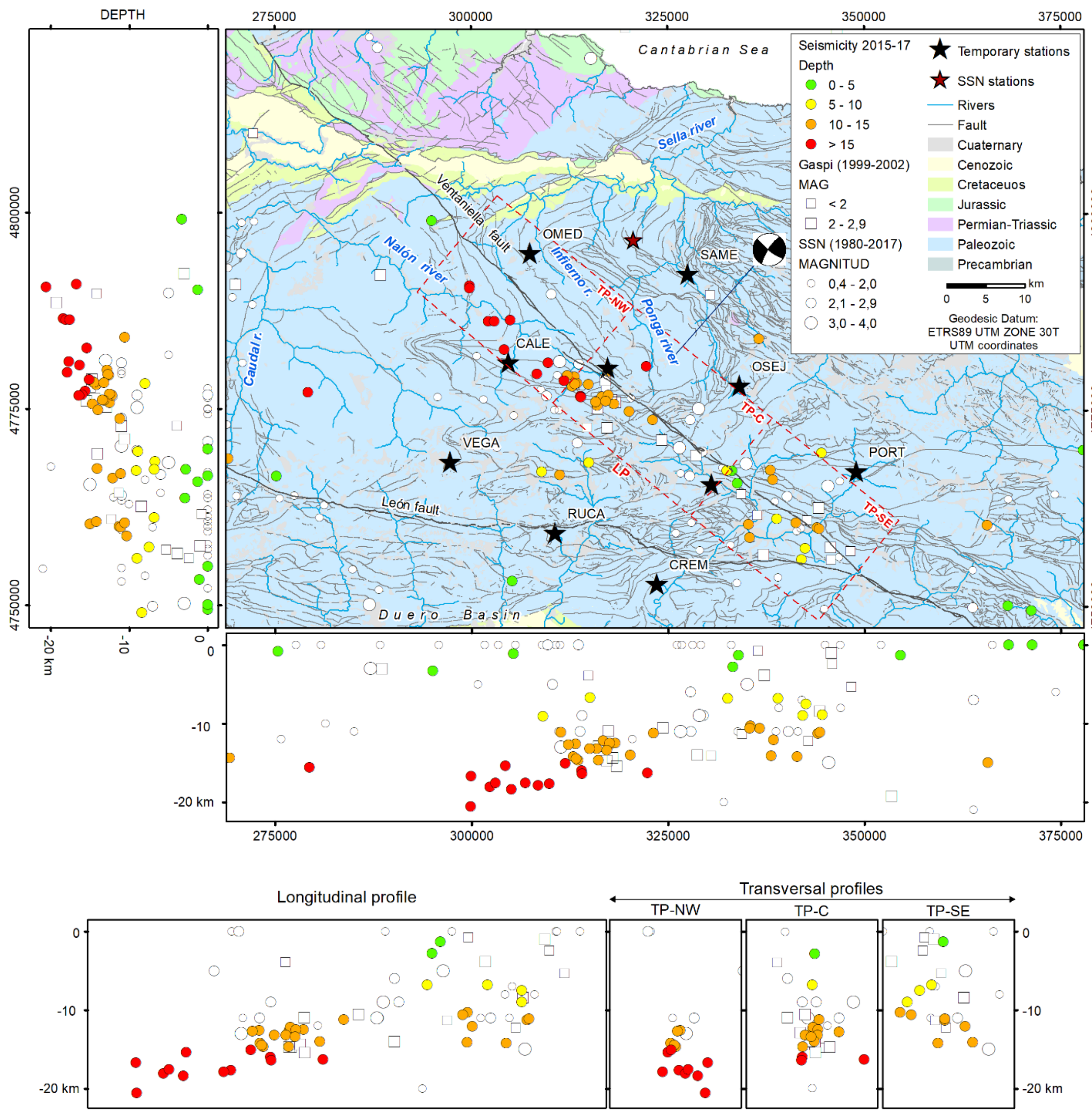

Figure 3. Map showing the location of the stations belonging to the portable seismic network of Ventaniella (black stars). Also represented are the dots indicating previous instrumental seismicity (empty circles) and activity registered by the network (solid circles). The focal mechanism shown in the figure corresponds to the largest earthquake registered (20/02/1989, m_bLg 3.7, Herráiz et al., 2000). In the lower part the projection of the events, there is a longitudinal profile along the fault

(represented by three dashed red boxes on the map) and three cross sections to the fault (NW, central and SE).

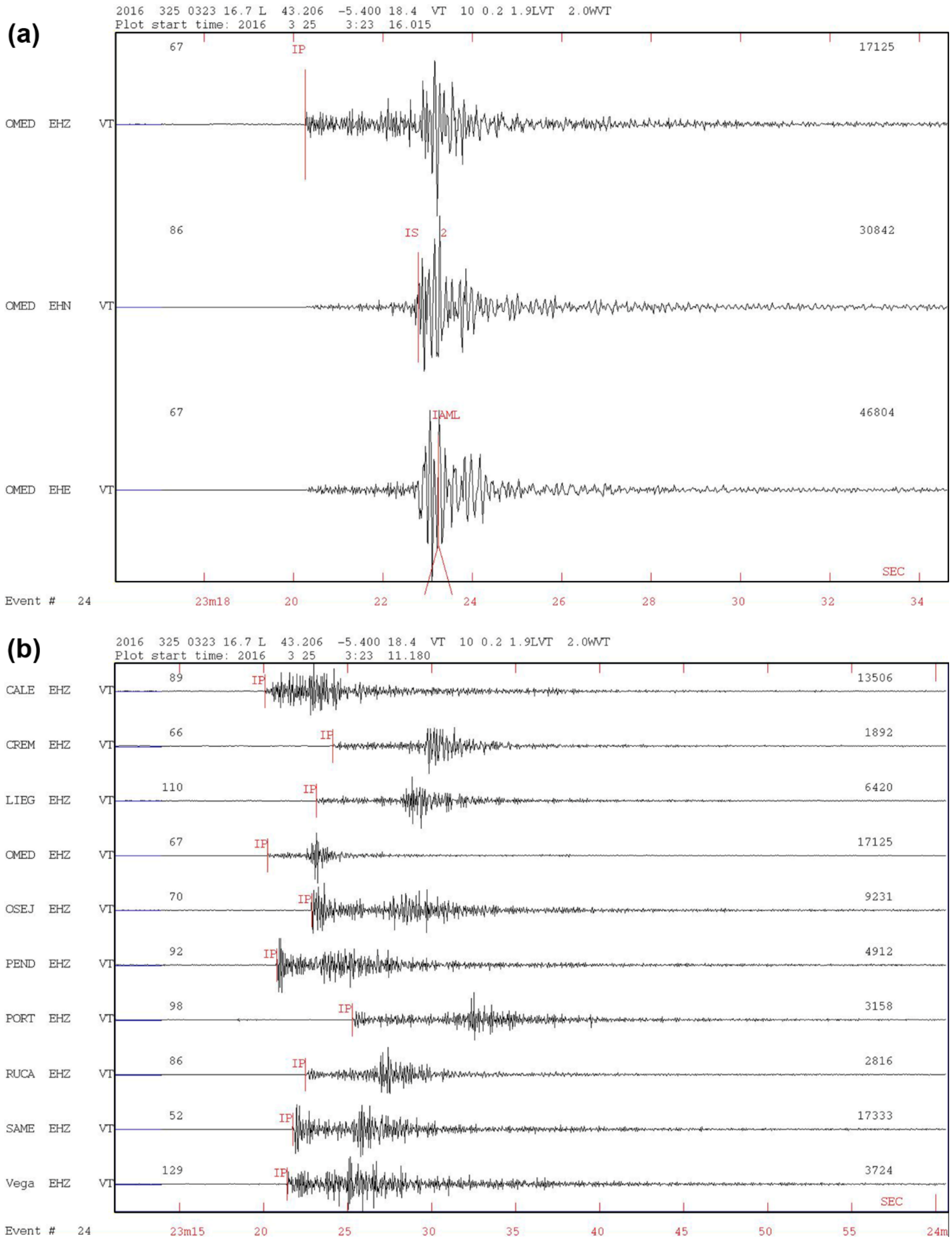

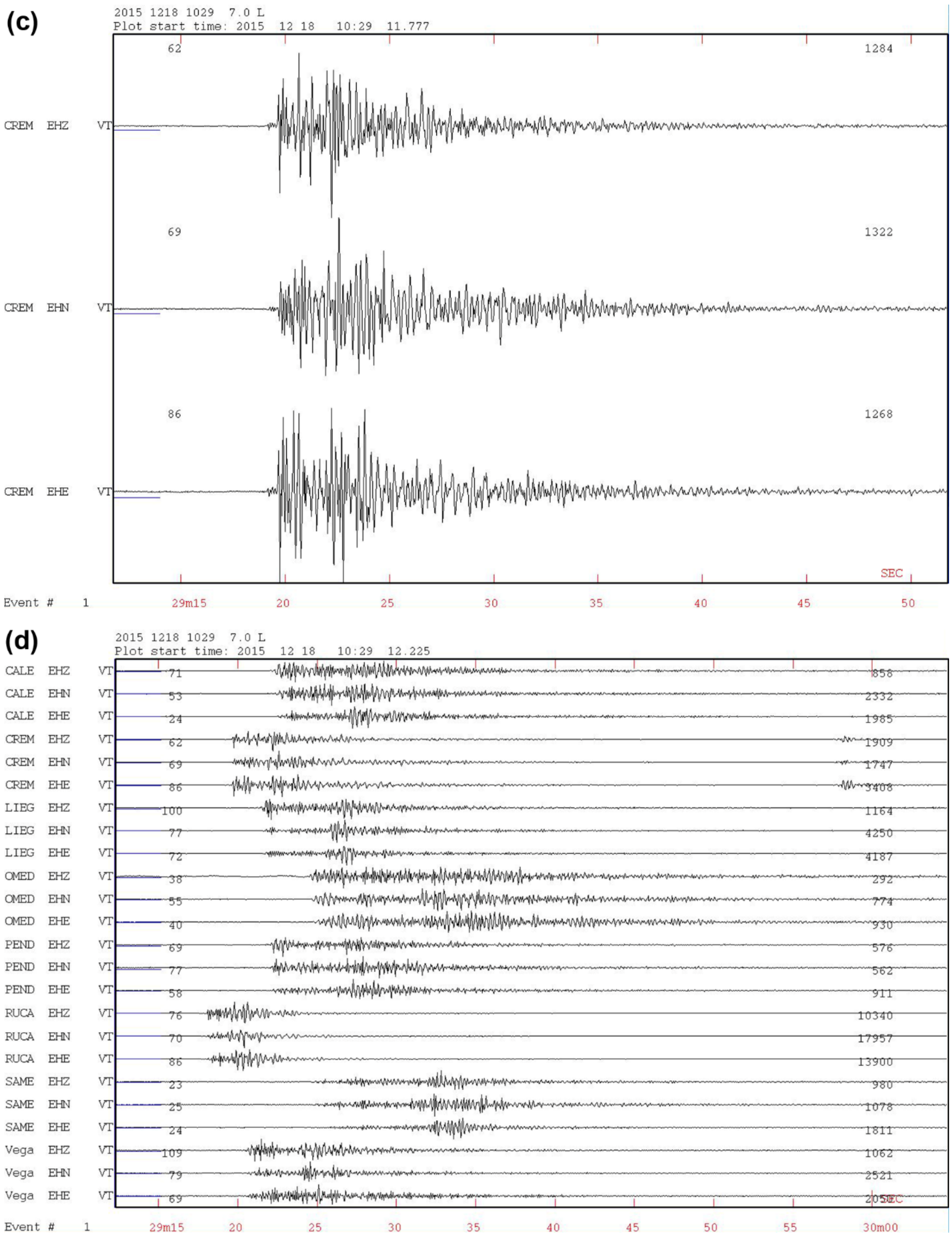

Figure 4. (a) Example of a seismogram recorded at the CALE station. (b) Image of the vertical canals at all stations during the largest earthquake recorded by the network (03/25/2016; Mw=2.0) in the vicinity of the Ventaniella Fault; first P and S waves have been identified on the

seismograms. (c) Characteristic signal produced by a quarry blast registered at the CREM Station on 12/18/2015 with epicenter at 16 km. (d) Record of the same event seen in 8 stations.

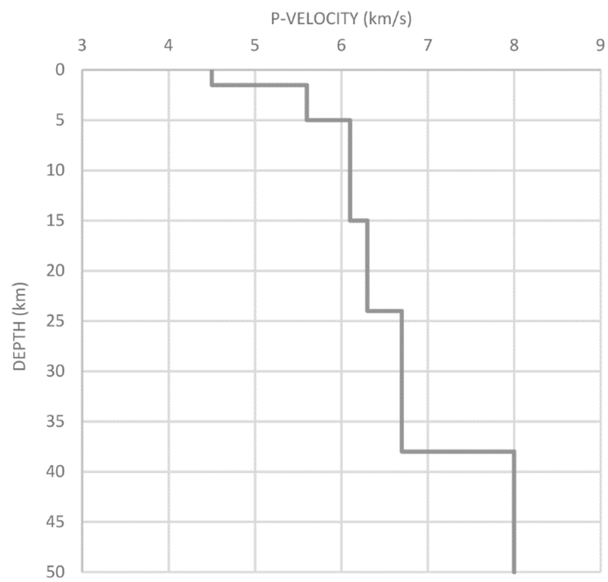

Figure 5. 1D velocity model used for the hypocentral determinations, based on Vp velocities obtained in refraction profiles through the study area by Fernández-Viejo et al. (2000).

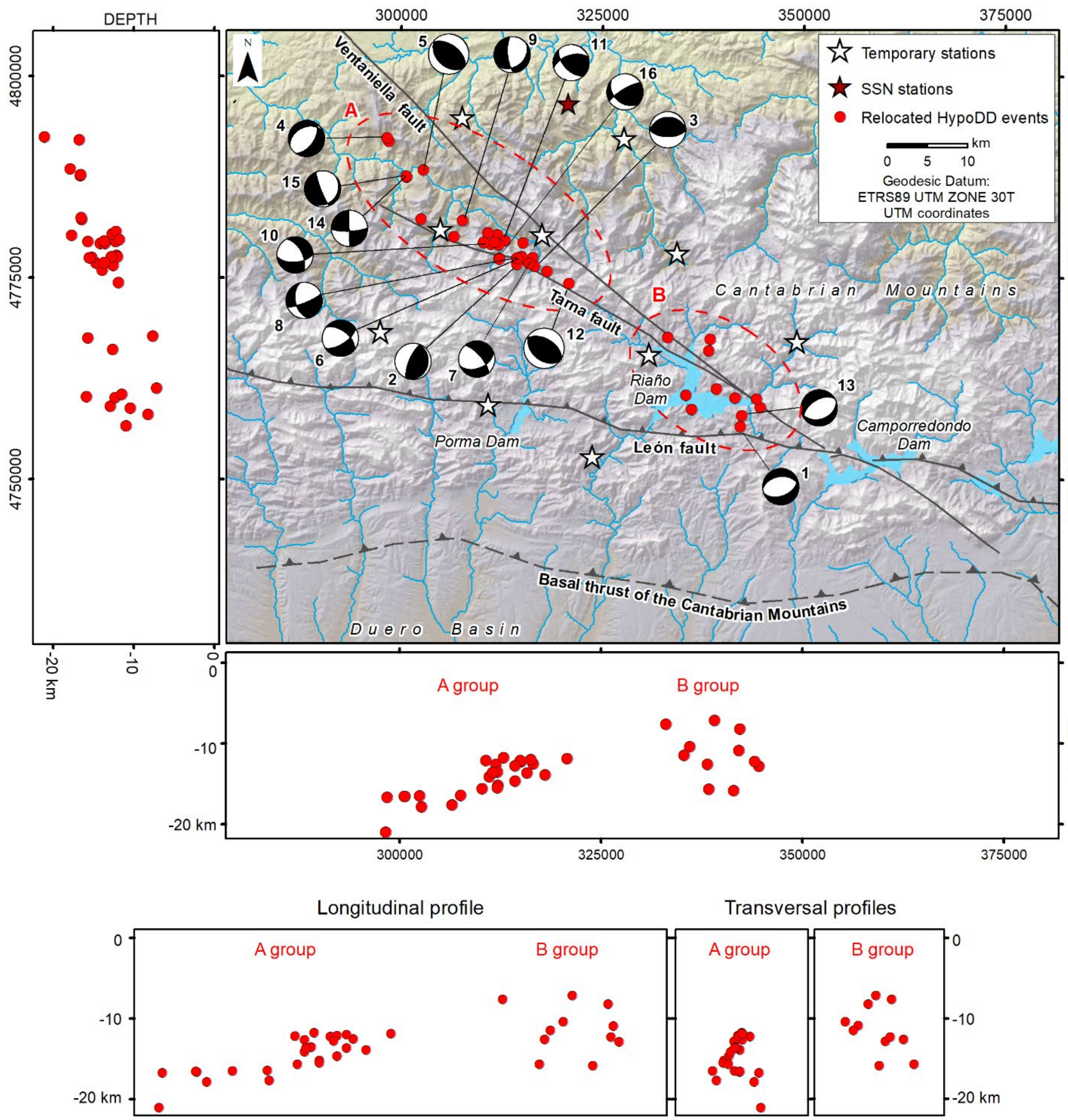

Figure 6. Map showing the distribution of seismic events after relocation with the double difference technique. 16 focal mechanisms obtained for selected events (see text) are also shown. The focal parameters for the 16 events are listed in Table 3. In the lower part, the projection of the earthquakes in a longitudinal profile to the fault and the cross sections to the fault for A and B subgroups are shown.

(a)

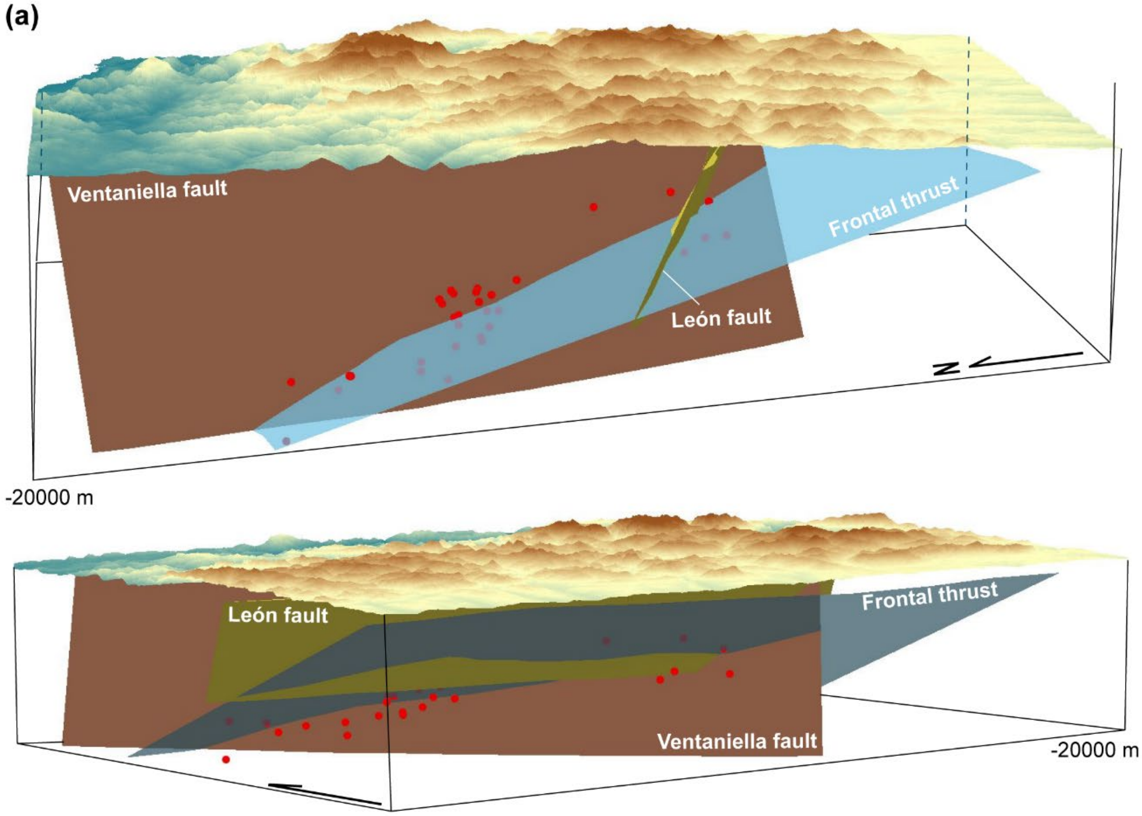

Ventaniella fault
Frontal thrust
León fault
N
-20000 m
León fault
Frontal thrust
Ventaniella fault
-20000 m

(b)

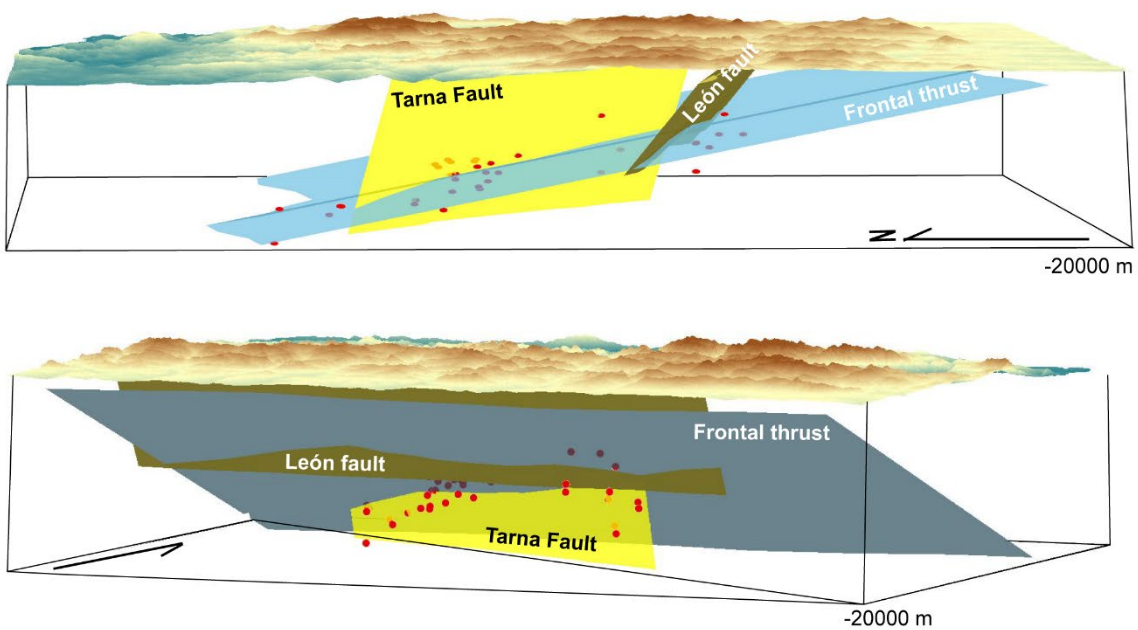

Tarna Fault
León fault
Frontal thrust
N
-20000 m
Frontal thrust
León fault
Tarna Fault
-20000 m

826

Figure 7. 3D Block diagrams illustrating the fault intersections proposed in the text to explain the seismicity recorded. The width of the fault zones is not truly represented, the faults are drawed as simple two dimensional planes. Events located in the “visible side” of the plane are in bright red, events in the “non visible” side in darker red. a) Diagram that shows the intersection between the Ventaniella Fault plane (solid brown) and the frontal thrust of the Cantabrian Mountains (translucid light blue), considering dips of 76˚SW and 20˚N respectively looking from the West and from the Southwest. (b) Sketch showing the intersection between the Tarna Fault (translucid yellow) and the León Fault plane (in dark green), the frontal thrust is shown for reference in translucid light blue.